

# Mechanoelectric Feedback in a Model of the Passively Inflated Left Ventricle

FREDERICK J. VETTER and ANDREW D. MCCULLOCH

Department of Bioengineering, University of California, San Diego, San Diego, CA

(Received 19 July 2000; accepted 7 February 2001)

**Abstract**—Mechanoelectric feedback has been described in isolated cells and intact ventricular myocardium, but the mechanical stimulus that governs mechanosensitive channel activity in intact tissue is unknown. To study the interaction of myocardial mechanics and electrophysiology in multiple dimensions, we used a finite element model of the rabbit ventricles to simulate electrical propagation through passively loaded myocardium. Electrical propagation was simulated using the collocation-Galerkin finite element method. A stretch-dependent current was added in parallel to the ionic currents in the Beeler–Reuter ventricular action potential model. We investigated different mechanical coupling parameters to simulate stretch-dependent conductance modulated by either fiber strain, cross-fiber strain, or a combination of the two. In response to pressure loading, the conductance model governed by fiber strain alone reproduced the epicardial decrease in action potential amplitude as observed in experimental preparations of the passively loaded rabbit heart. The model governed by only cross-fiber strain reproduced the transmural gradient in action potential amplitude as observed in working canine heart experiments, but failed to predict a sufficient decrease in amplitude at the epicardium. Only the model governed by both fiber and cross-fiber strain reproduced the epicardial and transmural changes in action potential amplitude similar to experimental observations. In addition, dispersion of action potential duration nearly doubled with the same model. These results suggest that changes in action potential characteristics may be due not only to length changes along the long axis direction of the myofiber, but also due to deformation in the plane transverse to the fiber axis. The model provides a framework for investigating how cellular biophysics affect the function of the intact ventricles. © 2001 Biomedical Engineering Society.

[DOI: 10.1114/1.1366670]

**Keywords**—Action potential morphology, Cardiac mechanics, Mechanosensitive channel, Stretch-dependent current, Excitation–contraction coupling, Numerical model study.

## INTRODUCTION

Little is known about how mechanical deformation affects action potential characteristics in the intact ven-

tricle. The three-dimensional anatomy of the ventricle and heterogeneity of regional strains are likely to affect the heterogeneity of electrical activation and repolarization. Under conditions of increased mechanical heterogeneity, mechanoelectric feedback may increase dispersion of repolarization or the likelihood of unidirectional block and consequent risk of reentrant arrhythmia.<sup>42</sup> Previous investigators have studied either regional strains<sup>30</sup> or action potential changes<sup>15,50</sup> during passive filling of the left ventricle (LV), but the relationships between three-dimensional regional deformations and action potential morphology have not been explored.

In the isolated Langendorff-perfused rabbit heart, Franz *et al.*<sup>15</sup> reported that resting potential increases at the epicardium and endocardium under sustained volume loading of the LV, while the action potential amplitude decreases. They also observed that the LV can be mechanically paced by transient 50 ms volume pulses of approximately 700  $\mu\text{L}$ . In isolated buffer-perfused canine hearts, Hansen *et al.*<sup>20</sup> measured the probability of eliciting a stretch-induced arrhythmia as a function of the magnitude of a 50 ms volume pulse; with a baseline volume of 20 mL the mean volume transient needed to cause a stretch-induced arrhythmia with at least 90% probability was  $21.3 \pm 8.5$  mL. Zabel *et al.*<sup>50</sup> showed the action potential amplitude decreased to  $72.3\% \pm 15\%$  of baseline when the LV was stretched to 175% of the baseline volume. In another study they reported that dispersion of action potential duration increased with a sustained increase in LV volume.<sup>51</sup> In the anesthetized canine, Lekven *et al.*<sup>26</sup> showed a transmurally nonuniform reduction in unipolar potential in response to increases in LV diameter. Infusion of 0.5–2.5 L of warm blood into the jugular vein resulted in an 11% increase in LV end-diastolic diameter and a corresponding 27% decrease in endocardial potential and a 15% decrease in epicardial potential.

Many investigators have hypothesized that mechanosensitive channels play a primary role in modifying action potential characteristics under LV volume loading.<sup>15,20,50</sup> Though most investigations have assumed

---

Address correspondence to Andrew D. McCulloch, Department of Bioengineering, University of California, San Diego, 9500 Gilman Drive, La Jolla, CA 92093-0412. Electronic mail: amcculloch@ucsd.edu

Frederick J. Vetter is currently with the Department of Pharmacology, SUNY Upstate Medical University, Syracuse, NY.

that changes in sarcomere or myofiber length is the governing mechanical stimulus, strain in the intact ventricle is nonuniform and deformation occurs in all dimensions.<sup>30</sup> In the unloaded state, three-dimensional residual strains also exist and have been reported in the rat, rabbit, and canine LV.<sup>10,16,29</sup> Regional LV strains exhibit complex three-dimensional alterations under ischemic conditions or the presence of an infarct.<sup>17,43</sup>

One-dimensional models based on the change in sarcomere length or circumferential strain have been useful for describing the qualitative effects of mechanosensitive channels in the myocardium. Zabel *et al.*<sup>50</sup> modeled cellular changes in action potential morphology observed in the rabbit heart using a stretch-dependent current model proposed by Sachs,<sup>40</sup> and found similarities between their model and observations of action potential changes at the epicardium of the isolated rabbit LV. Riemer *et al.*<sup>34</sup> examined the influence of the conductance and reverse potential of a mechanosensitive channel in two models of ventricular action potential. Using a model of the frog ventricular action potential, they found that action potential duration consistently shortens with reverse potentials of  $-20$  and  $-50$  mV; a guinea pig model also shows shorter duration action potentials with a  $-50$  mV reverse potential, but the duration lengthens with a  $-20$  mV reverse potential. Rice *et al.*<sup>33</sup> simulated the effect of circumferential lengthening during end systole in an ischemic region on the LV using magnetic resonance imaging with cardiac tagging. They found that the minimum stretch-dependent conductance needed to generate an action potential decreases as the number of abnormally stretched cells increases, suggesting that a very small number of cells could generate stretch-induced action potentials possibly resulting in a reentrant arrhythmia.

The objective of this study was to analyze the effect of regionally heterogeneous diastolic strains on action potential amplitude. We used a transmural plane from a three-dimensional model of the passively inflated rabbit ventricles as the computational domain.<sup>45</sup> The corresponding strains were used as the mechanical stimuli. To investigate the possible effects of mechanical heterogeneity, two models of the stretch-dependent conductance were considered. The first model used a fixed, spatially uniform conductance to generate a stretch-dependent current of uniform magnitude over the plane. The second model used strains from the model of the passively inflated ventricles to generate a transmembrane current modulated by the local strains in the deformed myocardium. We hypothesized that multiple components of myocardial deformation are the primary mechanical stimulus. Transmembrane current from the latter model varied regionally due to local variations in strain.

## METHODS

### *Anatomic Model*

The finite element model of rabbit ventricular geometry and myofiber architecture has been described previously.<sup>44</sup> Briefly, bicubic Hermite surfaces were fitted to over 8000 geometric coordinates measured from the epicardial and endocardial surfaces of a 9.0 g New Zealand White rabbit heart. Over 14,000 fiber orientation measurements were collected from transmural serial sections of the same heart; a mathematical description of the fiber angle orientation was formulated by fitting bilinear-cubic Hermite basis functions to the measured fiber angles. The resulting 36-element three-dimensional anatomic model of the ventricles has 552 degrees of freedom (DOF) and a root-mean-squared error (RMSE) of  $\pm 0.55$  mm (Fig. 1, left). The fitted fiber angle functions have 182 DOF and a RMSE of  $\pm 19^\circ$ .

In a subsequent study, we used the three-dimensional anatomic model to simulate the deformation of the rabbit ventricles during inflation.<sup>45</sup> Our estimates of the nonlinear, anisotropic material properties of resting rabbit ventricular myocardium resulted in a mechanics model with fiber and cross-fiber epicardial strains that agreed well with experimental observations. In this study we use these model strains at various LV pressures as realistic mechanical stimuli for stretch-dependent transmembrane currents.

To generate the computational domain for action potential propagation, we extracted two three-dimensional finite elements from the anterolateral wall and refined them in the circumferential, longitudinal, and transmural directions to generate a block (8 circumferential  $\times$  8 longitudinal  $\times$  8 transmural elements) with a spatial discretization of approximately 1 mm (Fig. 1, center). A transmural plane was then extracted from the block, resulting in a finite element mesh with 64 elements and 81 nodes (Fig. 1, right). Cubic Hermite interpolation of the planar geometry used two Gauss points in either local finite element direction.

### *Ionic and Stretch-Dependent Current Models*

The Beeler–Reuter model of ventricular action potential was used to model ionic transmembrane currents.<sup>3</sup> Mechanoelectric feedback in the model was incorporated by defining an additional transmembrane current to represent the current flowing through mechanosensitive channels. The magnitude of stretch-dependent current was governed by the reverse potential of the channel and a conductance modulated as a linear function of the material strain in the myocardium.<sup>33,34</sup> The stretch-dependent current and conductance had the form

$$I_{ms} = g_{ms}(V_m - V_r), \quad (1)$$

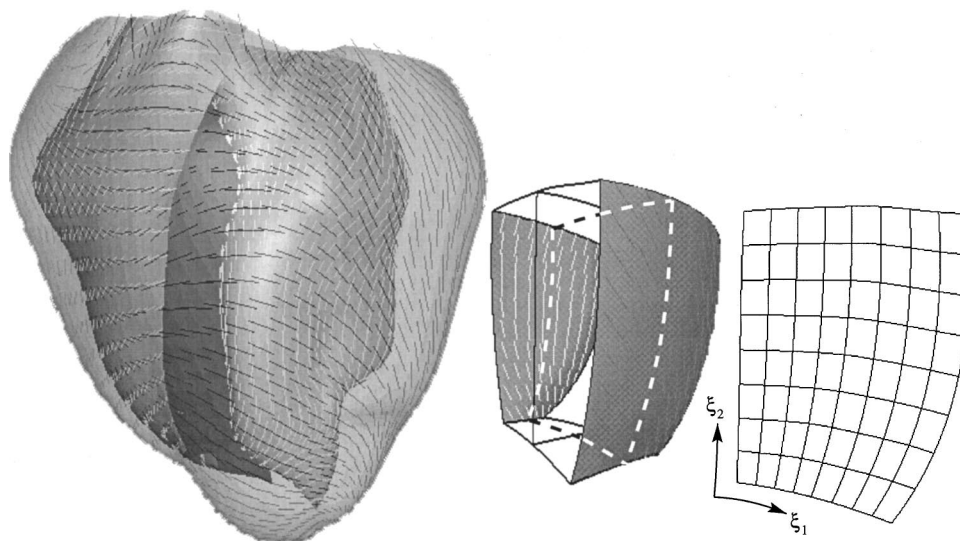


FIGURE 1. Generation of the propagation domain from the three-dimensional anatomic model. The ventricular model (left) was used in a previous study to simulate myocardial deformation over a range of LV cavity pressures (see Ref. 45). From a region in the anterolateral wall (center), a transmural plane was extracted for use as the computational domain in the current study (right). Dashed lines indicate boundaries of the transmural plane within the block. Local finite element coordinate directions indicate the transmural ( $\xi_1$ ) and longitudinal ( $\xi_2$ ) directions on the whole heart.

$$g_{ms} = G_{ms}(\alpha E + \beta), \quad (2)$$

where  $V_m$  is the transmembrane voltage (mV),  $I_{ms}$  is the stretch-dependent transmembrane current ( $\mu\text{A}/\text{cm}^2$ ),  $G_{ms}$  is the saturation conductance of the mechanosensitive channel ( $\text{mS}/\text{cm}^2$ ),  $E$  is the local value of either the fiber or cross-fiber strain, and  $\alpha$  is a dimensionless sensitivity parameter governing the magnitude of the mechanically modulated conductance. The scaling parameter  $\beta$  was constant throughout the tissue at any given mechanical state. We investigated the effects of a spatially uniform stretch-dependent conductance (i.e.,  $\alpha=0$  and  $\beta \neq 0$ ) and a stretch-dependent conductance that varied according to regional myocardial strain ( $\alpha \neq 0$ ). For all simulations the reverse potential ( $V_r$ ) was  $-20$  mV.<sup>11,22</sup>

*Spatially Uniform Stretch-Dependent Conductance.* First we examined action potential amplitude in response to a spatially uniform stretch-dependent conductance, i.e., the change in action potential due to a constant stretch-dependent conductance in the transmural plane. Experimental observations of single-channel conductances and densities<sup>22,24,38,41</sup> in the cell membrane suggest that mechanosensitive conductance ranges from  $0.21$  to  $19$   $\text{mS}/\text{cm}^2$ . Our preliminary studies showed that a mechanosensitive conductance of  $30$   $\text{mS}/\text{cm}^2$  blocked propagation of the action potential (as described in the Results section); hence, we used  $30$   $\text{mS}/\text{cm}^2$  as a limiting value of the mechanosensitive conductance in our model. In these simulations, the sensitivity parameter  $\alpha$  was

zero, the scaling parameter  $\beta$  was unity, and the stretch-dependent conductance ( $g_{ms}$ ) had a constant value of  $5$ ,  $10$ ,  $20$ ,  $25$ ,  $27.5$ , or  $30$   $\text{mS}/\text{cm}^2$ , with no influence of the regionally varying strains. An additional simulation with no stretch-dependent current ( $g_{ms}=0$ ) served as a baseline for comparison.

*Regionally Varying Stretch-Dependent Conductance.* Next, we investigated the effect of realistic heterogeneous myocardial strains on action potential amplitude. The stretch-dependent conductance was modulated by either regional fiber strain, cross-fiber strain, or a combination of the two. Table 1 shows the parameters used in each of the three models for  $g_{ms}$ , where  $E_{ff}$  is the fiber strain,  $E_{cc}$  is the cross-fiber strain, and  $\bar{E}_{ff}$  is the mean fiber strain (referred to the unloaded state) on the transmural plane. The values of the sensitivity parameter

TABLE 1. Different models of mechanosensitive conductance utilizing either fiber strain ( $E_{ff}$ ), cross-fiber strain ( $E_{cc}$ ), or cross-fiber and mean fiber strain ( $\bar{E}_{ff}$ ) as the mechanical stimulus. The conductivity  $G_{ms}$  is in  $\text{mS}/\text{cm}^2$ , the strain  $E$  and parameters  $\alpha$  and  $\gamma$  are dimensionless, with  $\gamma=1.74265$ . The values of the parameter were chosen such that the maximum value of the stretch-dependent conductance  $g_{ms}$  was  $30$   $\text{mS}/\text{cm}^2$  at  $15$  mm Hg pressure.

Model	$G_{ms}$	$E$	$\alpha$	$\beta$
$g_{ms}(E_{ff})$	200	$E_{ff}$	1.3995	0
$g_{ms}(E_{cc})$	200	$E_{cc}$	0.5045	0
$g_{ms}(E_{ff}, E_{cc})$	200	$E_{cc}$	0.1683	$\gamma \bar{E}_{ff}$

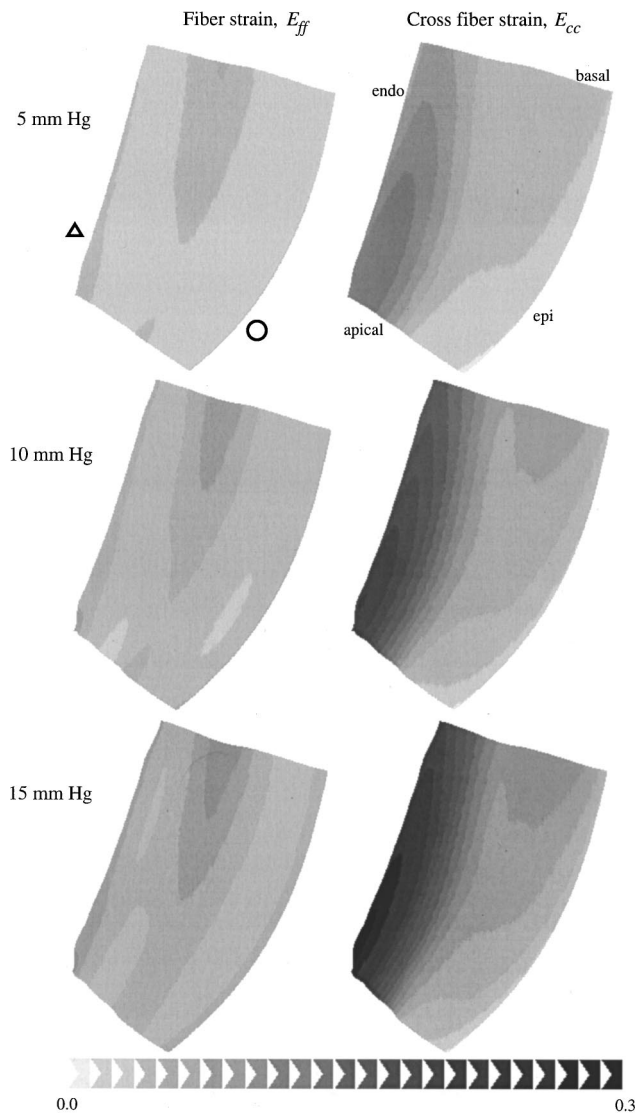


**FIGURE 2.** Maps of fiber and cross-fiber strain on the transmural plane as computed in a previous study of LV deformation under passive loading (see Ref. 45). Cross-fiber strain (right column) shows a distinct transmural gradient from epicardium to endocardium. Symbols  $\Delta$  and  $\circ$  identify endocardial and epicardial locations where action potential amplitude ratios were computed. All images show the geometry at the same scale; note that the plane narrows in the transmural direction with increasing pressure, consistent with LV wall thinning during diastole.

$\alpha$  and scaling parameter  $\gamma$  were chosen such that at a LV cavity pressure of 15 mm Hg the maximum value of  $g_{ms}$  was  $30 \text{ mS/cm}^2$ —the limiting value described above—on the transmural plane. The fiber or cross-fiber strains used as the mechanical stimulus for this conductance model were the strains resulting from simulations of passive LV inflation.<sup>45</sup> The strains on the transmural plane are shown in Fig. 2; the minimum fiber strain at 5 mm Hg LV pressure was 0.016. The minimum cross-fiber strain at 5 mm Hg was 0.015. At 15 mm Hg, note that the fiber

strain was more homogeneous (varying from 0.036 to 0.097) than the cross-fiber strain, which showed a substantial transmural gradient from epicardium (0.026) to endocardium (0.289) at 15 mm Hg.

### Two-Dimensional Propagation

The myocardium was approximated as a continuum in which propagation is governed by the two-dimensional cable equation. The coefficients of the conductivity tensor were estimated in a three-dimensional model.<sup>46</sup> The conductivity in the transmural plane was assumed to be constant and approximated with an isotropic conductivity tensor with values of the conductivity transverse to the long axis of the myofiber. Thus, the diagonal components of the conductivity tensor were  $0.565 \text{ mS/cm}$  and the off-diagonal components were zero. The membrane capacitance was  $1.0 \mu\text{F/cm}^2$  and  $2000 \text{ cm}^{-1}$  was used as the cell surface-to-volume ratio.<sup>31</sup>

The collocation-Galerkin finite element method was used to solve the discretized cable equation with no-flux boundary conditions.<sup>37</sup> In all of the simulations, the time- and voltage-dependent variables of the ionic current model were brought to their quiescent state by simulating the first 400 ms with no applied stimulus. Then, the ventricular action potential was initiated with a 4 ms threshold stimulus applied to the nodes along the most basal edge of the two-dimensional transmural plane. All runs simulated 900 ms. The time history of transmembrane voltage was recorded at  $100 \mu\text{s}$  intervals for later analysis and visualization. The ordinary differential equations describing the state variables in the Beeler-Reuter model were integrated using an implicit Adams method with  $10^{-4}$  relative and absolute error tolerances.<sup>21</sup> The resting transmembrane potential was defined as the value 5 ms before the stimulus was applied, and the action potential amplitude was defined as the difference between the maximal voltage during the plateau phase (the “dome” voltage) and the resting transmembrane potential, similar to experimental protocols using monophasic action potential electrode recordings.<sup>14</sup> Action potential duration at 90% repolarization ( $\text{APD}_{90}$ ) was calculated as the time elapsed from the maximum rate of action potential upstroke to the point of 90% repolarization from the action potential amplitude. Dispersion of action potential duration was calculated as the absolute value of difference in  $\text{APD}_{90}$  at the locations of maximum and minimum mechanosensitive conductance on the plane. The ratios of loaded (LV cavity pressure of 5, 10, or 15 mm Hg) to baseline (no stretch-dependent current) action potential amplitudes were computed at points on the endocardium and epicardium located approximately 4.25 mm from the stimulus region (identified by the symbols  $\Delta$  and  $\circ$  in Fig. 2). All simulations were run on a SGI Octane work station

**TABLE 2. Resting membrane potential and action potential amplitude and duration for a spatially uniform stretch-dependent conductance. Plots are shown in Fig. 3. Conductance ( $g_{ms}$ ) is in  $\text{mS}/\text{cm}^2$ , resting membrane potential ( $V_{RMP}$ ) and amplitude in millivolts, and action potential duration ( $APD_{90}$ ) in milliseconds. Amplitude for the  $g_{ms}=27.5$   $\text{mS}/\text{cm}^2$  simulation was computed from the maximum potential of the upstroke. Propagation failed for the  $g_{ms}=30$   $\text{mS}/\text{cm}^2$  simulation.**

$g_{ms}$	0	5	10	20	25	27.5	30
$V_{RMP}$	-84.6	-82.6	-80.4	-75.8	-73.3	-72.0	-70.6
Amplitude	100.0	96.1	92.0	81.9	69.3	48.0	...
$APD_{90}$	287.3	288.3	289.7	293.7	300.0	...	...

with a 225 MHz MIPS R10000 processor and 1664 Mb of main memory. Each simulation solved for 2592 degrees of freedom and typically required 20 min to complete. The program and data required 28.3 and 17.7 Mb of main memory, respectively.

## RESULTS

### *Spatially Uniform Stretch-Dependent Conductance*

The resting potential and action potential amplitude for the baseline and five spatially uniform stretch-dependent conductance simulations are shown in Table 2. The baseline ( $g_{ms}=0$ ) resting transmembrane potential was  $-84.6$  mV, the maximum amplitude was 16.3 mV at the peak of the upstroke and 15.5 during the plateau phase (Fig. 3); the action potential duration at 90% repolarization ( $APD_{90}$ ) was 287.3 ms. When the conductance ranged from 5 to 30  $\text{mS}/\text{cm}^2$  the maximum amplitude of both the upstroke and plateau decreased; with a conductance of 25  $\text{mS}/\text{cm}^2$  the upstroke and plateau amplitudes decreased to 65% and 69% of the baseline, respectively.  $APD_{90}$  increased nonlinearly with the

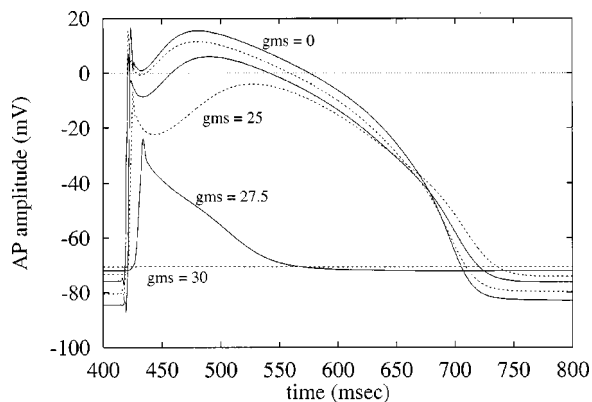


**FIGURE 3. Action potentials from the endocardial surface using a spatially uniform stretch current [i.e.,  $\alpha=0$ ,  $\beta=1$  in Eq. (2)]. For the plots shown, the stretch-dependent conductance  $g_{ms}$  was 0, 10, 20, 25, 27.5, or 30  $\text{mS}/\text{cm}^2$ . The plot for  $g_{ms}=5$   $\text{mS}/\text{cm}^2$  is not shown for clarity. Note that action potential propagation failed when  $g_{ms}=30$   $\text{mS}/\text{cm}^2$ .**

**TABLE 3. Variations of stretch-dependent conductance (mean $\pm$ SD  $\text{mS}/\text{cm}^2$ ) with LV pressure of the different stretch conductance models.**

LV Pressure	$g_{ms}(E_{ff})$		
	Min	Max	Mean $\pm$ SD
5 mm Hg	3.66	13.96	$7.12 \pm 2.25$
10 mm Hg	7.39	24.03	$12.81 \pm 3.42$
15 mm Hg	9.63	30.00	$16.46 \pm 4.09$
LV Pressure	$g_{ms}(E_{cc})$		
	Min	Max	Mean $\pm$ SD
5 mm Hg	0.84	12.86	$5.98 \pm 3.38$
10 mm Hg	1.33	23.24	$10.58 \pm 6.09$
15 mm Hg	1.52	30.00	$13.59 \pm 7.85$
LV Pressure	$g_{ms}(E_{ff}, E_{cc})$		
	Min	Max	Mean $\pm$ SD
5 mm Hg	9.58	13.59	$11.30 \pm 1.13$
10 mm Hg	16.19	23.50	$19.28 \pm 2.03$
15 mm Hg	20.51	30.00	$24.53 \pm 2.62$

conductance. The action potential failed to propagate when the conductance was 30  $\text{mS}/\text{cm}^2$ . The resting membrane potential ( $V_{RMP}$ ) decreased linearly with increasing conductance:

$$V_{RMP} = 0.467 g_{ms} - 84.9, \quad r^2 = 0.9985. \quad (3)$$

During repolarization the action potentials generated from a nonzero stretch conductance crossed over the baseline action potential between 22% and 41% baseline repolarization (i.e., between 669 and 693 ms in Fig. 3). Crossover time was inversely proportional to conductance: the earliest crossover occurred with  $g_{ms} = 25$   $\text{mS}/\text{cm}^2$ , and the latest with  $g_{ms} = 5$   $\text{mS}/\text{cm}^2$ . The potential at which the crossover occurred ranged from  $-57$  to  $-37$  mV. The lowest conductance (5  $\text{mS}/\text{cm}^2$ ) had the most negative crossover potential ( $-57$  mV), and the crossover potential became less negative with increasing conductances. The crossover potential was always more negative than the reverse potential of the mechanosensitive channel.

### *Regionally Varying Stretch-Dependent Conductance*

Variations of the stretch-dependent conductance for the three  $g_{ms}$  models are listed in Table 3. All three models showed an increase in mean conductance with increasing left ventricular pressure. In none of the simulations was propagation blocked. Recall that the maximum conductance at 15 mm Hg for the three models was fixed at 30  $\text{mS}/\text{cm}^2$ . For the range of pressures simulated, the lowest mean and minimum conductances were al-

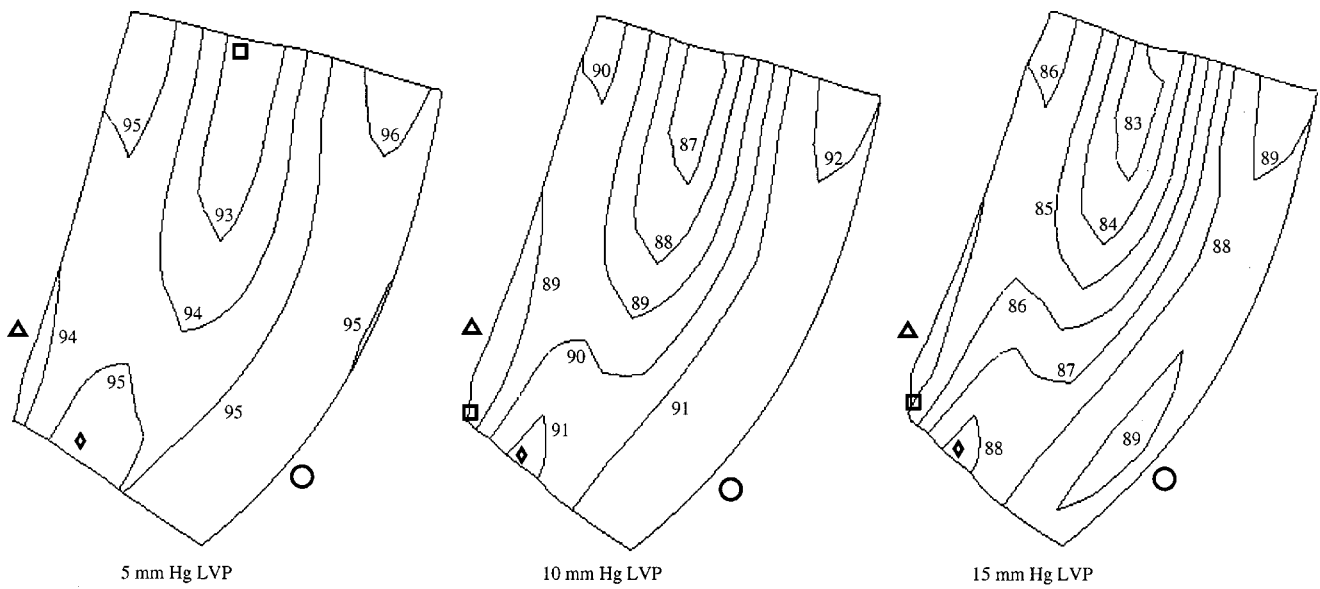


**FIGURE 4.** Maps of action potential amplitude at 5, 10, and 15 mm Hg LV pressure. Mechanosensitive conductance model was  $g_{ms}(E_{ff})$ . Contours are drawn at every 1 mV. Action potential amplitudes at the endocardium ( $\Delta$ ) and epicardium ( $\circ$ ) are listed in Table 6. Maximum ( $\square$ ) and minimum ( $\diamond$ ) conductances are listed in Table 3.

ways produced by the  $g_{ms}(E_{cc})$  model, and the largest produced by the  $g_{ms}(E_{ff}, E_{cc})$  model.

Figures 4–6 show the locations of the maximum ( $\square$ ) and minimum ( $\diamond$ ) conductances. For the  $g_{ms}(E_{ff})$  model (Fig. 4) the apical midwall location of the minimum conductance was unchanged over the range of LV pressures, but the location of the maximum conductance moved from the basal midwall at 5 mm Hg to the apical

subendocardium at higher pressures. Similarly, the apical subepicardial location of the minimum conductance for the  $g_{ms}(E_{cc})$  and  $g_{ms}(E_{ff}, E_{cc})$  models (Figs. 5 and 6) did not change over the pressure range. In both models, though, the maximum conductance location shifted slightly in the transmural direction toward the endocardium at pressures above 5 mm Hg, but maintained the same longitudinal position.

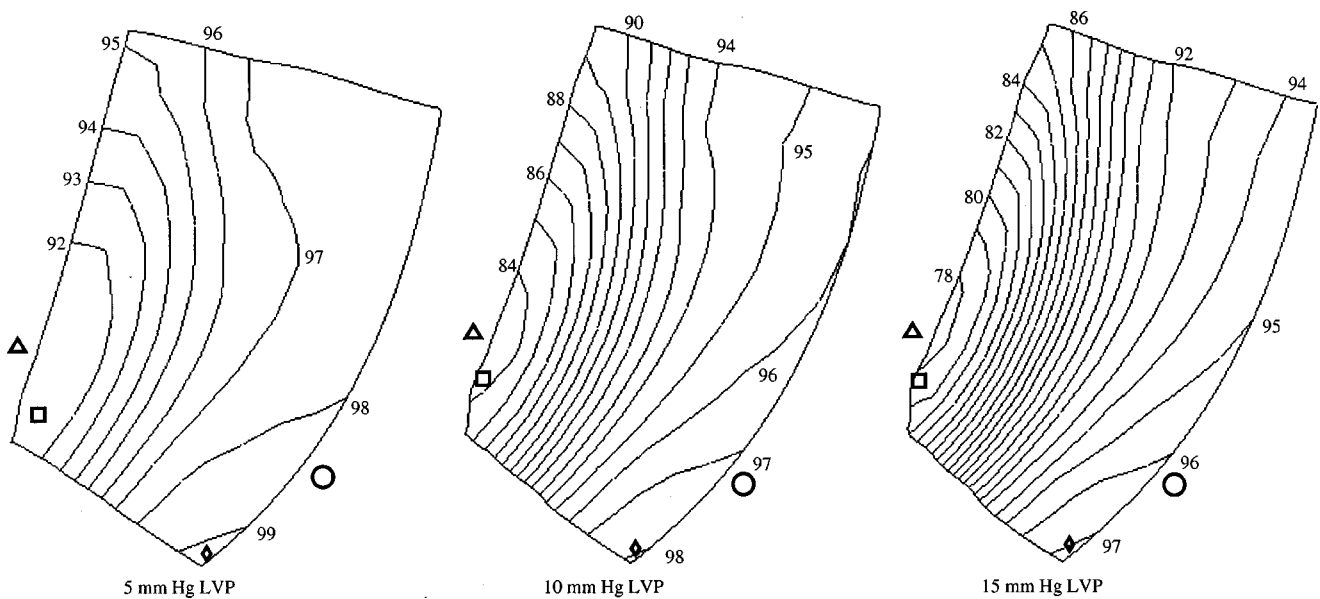


**FIGURE 5.** Maps of action potential amplitude at 5, 10, and 15 mm Hg LV pressure. Mechanosensitive conductance model was  $g_{ms}(E_{cc})$ . Contours are drawn at every 1 mV. Action potential amplitudes at the endocardium ( $\Delta$ ) and epicardium ( $\circ$ ) are listed in Table 6. Maximum ( $\square$ ) and minimum ( $\diamond$ ) conductances are listed in Table 3. Not all contours are labeled for clarity.

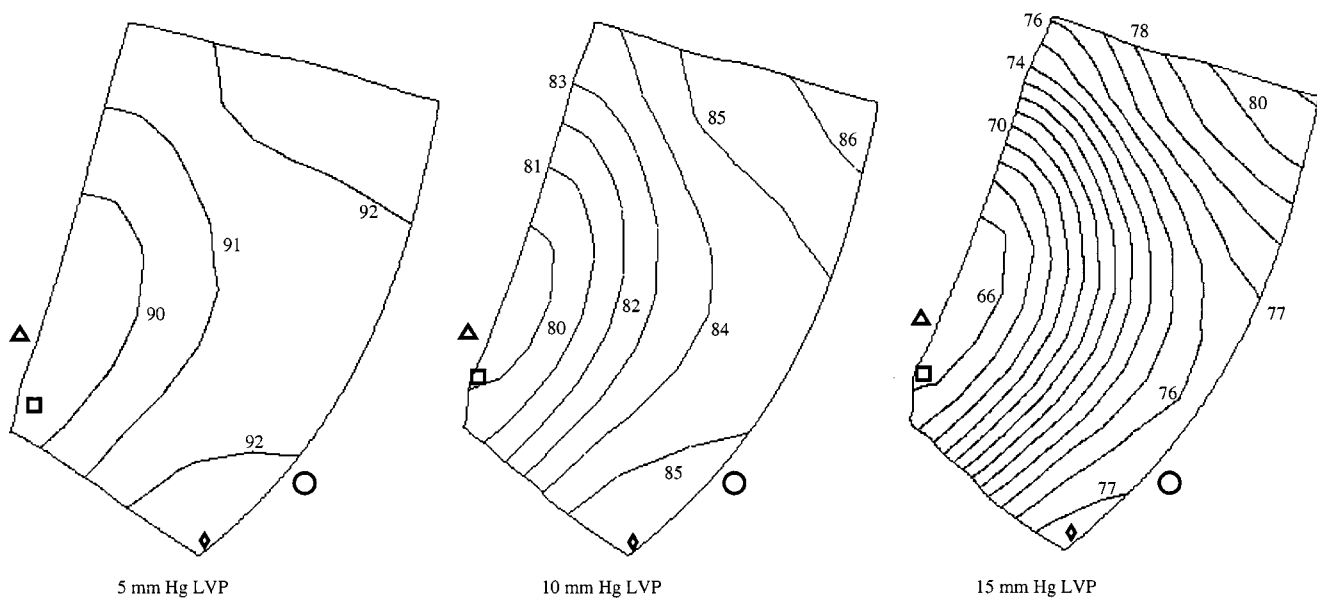


FIGURE 6. Maps of action potential amplitude at 5, 10, and 15 mm Hg LV pressure. Mechano-sensitive conductance model was  $g_{ms}(E_{ff}, E_{cc})$ . Contours are drawn at every 1 mV. Action potential amplitudes at the endocardium ( $\Delta$ ) and epicardium ( $\circ$ ) are listed in Table 6. Maximum ( $\square$ ) and minimum ( $\diamond$ ) conductances are listed in Table 3. Not all contours are labeled for clarity.

Dispersion of  $APD_{90}$  was computed at the locations of the maximum ( $\square$ ) and minimum ( $\diamond$ ) conductance (Table 4). For the  $g_{ms}(E_{ff})$  model dispersion of  $APD_{90}$  decreased with increasing pressure, ranging from 8.3 ms at 5 mm Hg to 1.1 ms at 15 mm Hg. Dispersion of  $APD_{90}$  for both the  $g_{ms}(E_{cc})$  and  $g_{ms}(E_{ff}, E_{cc})$  models increased from 5 to 15 mm Hg pressure, from 7.2 to 11.1 ms with the  $g_{ms}(E_{cc})$  model and from 4.6 to 9.0 ms with the  $g_{ms}(E_{ff}, E_{cc})$  model. The mean action potential amplitude for the three models of regionally varying stretch-dependent conductance (Table 5) was consistently less than the baseline (100 mV) but higher than the spatially uniform model with  $g_{ms} = 25 \text{ mS/cm}^2$  (69.3 mV). Over the entire range of LV pressures the standard deviation of the action potential amplitude was always lowest with the  $g_{ms}(E_{ff})$  model and largest with the  $g_{ms}(E_{cc})$  model.

At the endocardium, the  $g_{ms}(E_{ff})$  model consistently produced a larger action potential amplitude than the  $g_{ms}(E_{cc})$  model, which in turn was larger than that of the

$g_{ms}(E_{ff}, E_{cc})$  model (Table 6). At the epicardial site, the  $g_{ms}(E_{ff}, E_{cc})$  model still produced the lowest action potential amplitude, but the  $g_{ms}(E_{cc})$  model produced the largest.

When the stretch-dependent conductance was modulated by the regional strains, the action potential amplitude also varied spatially (Figs. 4–6). The action potential amplitudes at the endocardial and epicardial locations (labeled  $\Delta$  and  $\circ$  in Figs. 4–6) are shown in Table 6. Spatial variation of the action potential amplitude from the  $g_{ms}(E_{ff})$  and  $g_{ms}(E_{cc})$  models closely followed that of the fiber or cross-fiber strain, respectively, with smaller action potential amplitudes associated with higher strains and larger amplitudes associated with lower strains (Figs. 2, 4, and 5). For the  $g_{ms}(E_{ff})$  model the smallest action potential amplitude was located at the midwall, extending longitudinally from the basal boundary toward the apex; the largest amplitude was located at

TABLE 4. Dispersion of action potential duration at 90% repolarization (ms) at the locations of maximum ( $\square$ ) and minimum ( $\diamond$ ) conductance over the range of LV cavity pressures for the three models of regionally varying stretch-dependent conductance. Note that dispersion of  $APD_{90}$  decreases with increasing pressure using the  $g_{ms}(E_{ff})$  model, but increases using the other models.

	$g_{ms}(E_{ff})$	$g_{ms}(E_{cc})$	$g_{ms}(E_{ff}, E_{cc})$
5 mm Hg	8.3	7.2	4.6
10 mm Hg	1.2	10.2	5.5
15 mm Hg	1.1	11.1	9.0

TABLE 5. Action potential amplitude (mean  $\pm$  SD mV) over the range of LV cavity pressures for the three models of regionally varying stretch-dependent conductance. Note that all the amplitudes are less than 100 mV, the baseline amplitude with no stretch-dependent conductance (Table 2, second column), but greater than 69.3 mV, and the amplitude with a spatially uniform stretch-dependent conductance of 25  $\text{mS/cm}^2$  (Table 2, sixth column).

	$g_{ms}(E_{ff})$	$g_{ms}(E_{cc})$	$g_{ms}(E_{ff}, E_{cc})$
5 mm Hg	94.7 $\pm$ 0.9	95.6 $\pm$ 2.4	91.2 $\pm$ 1.0
10 mm Hg	90.0 $\pm$ 1.5	91.7 $\pm$ 4.4	83.4 $\pm$ 2.0
15 mm Hg	86.6 $\pm$ 1.9	88.7 $\pm$ 5.9	73.0 $\pm$ 4.7

**TABLE 6. Action potential amplitude (mV) at the endocardial ( $\Delta$ ) and epicardial ( $\circ$ ) locations in Figs. 4–6. The last column is the ratio of endocardial to epicardial action potential amplitude at the same LV cavity pressure.**

LV		$g_{ms}(E_{ff})$		
Pressure	Endo	Epi	Ratio	
5 mm Hg	93.8	95.2	0.985	
10 mm Hg	88.4	91.6	0.965	
15 mm Hg	84.6	88.8	0.953	
LV		$g_{ms}(E_{cc})$		
Pressure	Endo	Epi	Ratio	
5 mm Hg	91.0	98.5	0.924	
10 mm Hg	83.4	97.2	0.858	
15 mm Hg	77.5	96.2	0.806	
LV		$g_{ms}(E_{ff}, E_{cc})$		
Pressure	Endo	Epi	Ratio	
5 mm Hg	89.4	92.0	0.972	
10 mm Hg	79.5	85.2	0.933	
15 mm Hg	65.3	76.6	0.852	

the subepicardium, also extending from the basal boundary toward the apex. Results from the  $g_{ms}(E_{cc})$  model show a similar inverse relationship between action potential amplitude and cross-fiber strain. The smallest amplitude, like the largest cross-fiber strain, was consistently located near the apical boundary at the endocardium; the largest amplitude was at the apical boundary at the epicardium. A positive gradient in action potential amplitude extended transmurally from the endocardium toward the epicardium. The action potential amplitudes from the  $g_{ms}(E_{ff}, E_{cc})$  model showed characteristics similar to the amplitudes from both the  $g_{ms}(E_{ff})$  and  $g_{ms}(E_{cc})$  models. The largest amplitude was located at the epicardium, similar to the  $g_{ms}(E_{ff})$  model, but the spatial variation was oriented more in the transmural direction than longitudinally. Like the  $g_{ms}(E_{cc})$  model the smallest amplitude is near the apical boundary at the endocardium, and the gradient increases from endocardium to epicardium, though the gradient was most distinct at 15 mmHg. At lower pressures the action potential amplitudes appear more transmurally uniform, with a difference of approximately 2 mV across the wall at 5 mmHg.

## DISCUSSION

We have conducted simulations of the effects of regional transmural fiber and cross-fiber strain on the action potential amplitude in a realistically deformed model of the rabbit ventricles. The transmembrane voltage was simulated using the Beeler–Reuter model of ventricular action potential. To this we added a parallel transmem-

brane current with a stretch-dependent conductance. Two general models of stretch-dependent conductance were investigated: the first was a spatially constant conductance, the second was a regionally varying conductance modulated by heterogeneous myocardial strains.

### *Spatially Uniform Stretch-Dependent Conductance*

The linear relationship between the constant stretch-dependent current and the rest potential [Eq. (3)] is not surprising since the conductance model we used is Ohmic with no time dependence. The time of intersection between the stretched potentials and baseline occurred earlier and the potential increased with increasing  $g_{ms}$  (Fig. 3). The increasing potential with  $g_{ms}$  is to be expected because, once the transmembrane potential drops below the reverse potential of the stretch current a larger value of  $g_{ms}$  provides more inward current, slowing the rate of repolarization. That the intersection occurs earlier with increasing  $g_{ms}$  merely emphasizes the relative increase in repolarization rate. Similar to the findings reported by Zabel *et al.*,<sup>50</sup> the potential at which the action potential under stretch crosses the baseline action potential is lower than the reverse potential of the mechanosensitive channel. However, our results show the crossover potential becomes more positive with increasing stretch-dependent current, whereas no change in the crossover potential was reported by Zabel *et al.*<sup>50</sup> This is likely due to the different models of action potential and mechanosensitive conductance we used, although we would expect the variation in crossover potential to correlate with variations in stretch-dependent current. The variation in action potential amplitude provided by the spatially uniform stretch-dependent conductance is qualitatively similar to that measured in the rabbit heart,<sup>50</sup> but this model did not predict the transmural gradient in potential changes observed by Lekven *et al.*<sup>26</sup>

### *Regionally Varying Stretch-Dependent Conductance*

With the regionally varying stretch-dependent conductance model we examined three types of mechanical stimulus that may govern the mechanosensitive conductance. The model based on cross-fiber strain ( $E_{cc}$ ) stimulus always provided a lower minimum and mean conductance than the models based on either fiber strain ( $E_{ff}$ ) or the cross-fiber strain and mean-fiber strain ( $E_{cc}, \bar{E}_{ff}$ ) stimuli. This was not surprising since at the epicardium the cross-fiber strain was always less than the fiber strain over the range of LV pressures we examined (Fig. 2). Conversely, the maximum conductance was always provided by the fiber strain stimulus for LV pressures of 5 and 10 mmHg. This was unexpected since the fiber strain is less than the cross-fiber strain (at the en-

docardium) for the range of LV pressures. This may be due to the maximum  $30 \text{ mS/cm}^2$  value of the conductance established for the three models at 15 mm Hg. If the maximum conductance were established differently (e.g., set to the minimum value where propagation failed) the maximum conductance would likely be given by the cross-fiber strain stimulus instead of the fiber strain stimulus.

Using a Langendorff-perfused rabbit heart, Zabel *et al.*<sup>50</sup> applied a sustained 75% increase in LV volume which reduced the epicardial action potential amplitude to  $72.3\% \pm 15\%$  of the baseline. Lekven *et al.*,<sup>26</sup> using working canine hearts, increased LV end-diastolic diameter by 11% and measured reductions in the epicardial and endocardial unipolar potential to 85.3% and 72.2% of the baseline, respectively. As shown in Table 6, at 15 mm Hg the stretch-dependent conductance model based on fiber strain,  $g_{\text{ms}}(E_{\text{ff}})$ , reduced the epicardial action potential amplitude to 88.8% of the baseline; this is similar in magnitude to the reduction in epicardial potential reported by Lekven *et al.*,<sup>26</sup> but the model does not reproduce the transmural gradient, providing a reduction to only 84.6% at the endocardium. The conductance model based on cross-fiber strain,  $g_{\text{ms}}(E_{\text{cc}})$ , does reproduce the transmural gradient: epicardial and endocardial action potential amplitudes are reduced to 96.2% and 77.5% of the baseline, respectively. This model does not, however, show sufficient reduction in the action potential amplitude at the epicardium. Thus, either of the two stretch-dependent conductance models based exclusively on fiber strain or cross-fiber strain did not simultaneously reproduce the magnitude of reduction in the epicardial and endocardial action potential amplitudes observed experimentally. Only the model based on both fiber and cross-fiber strains resulted in a large reduction of the epicardial action potential amplitude with an even greater reduction of the endocardial potential. At the epicardium the  $g_{\text{ms}}(E_{\text{ff}}, E_{\text{cc}})$  model produced an action potential with 76.6% of the baseline amplitude, and a corresponding endocardial amplitude that was 65.3% of the baseline.

Zabel *et al.*,<sup>51</sup> using an isolated rabbit heart, reported that increasing left ventricular volume by 1 mL from a neutral volume increased the dispersion of  $\text{APD}_{70}$  from 27 to 38 ms on the epicardium. Similar to those measured results, the models based on either cross-fiber strain alone or both fiber strain and cross-fiber strain showed an increase in dispersion of  $\text{APD}_{90}$  with increasing LV pressure (and volume<sup>45</sup>). Dispersion of  $\text{APD}_{90}$  increased by 3.9 ms with the  $g_{\text{ms}}(E_{\text{cc}})$  model; the increase with the  $g_{\text{ms}}(E_{\text{ff}}, E_{\text{cc}})$  model was 4.4 ms (Table 4), or 96%. The discrepancy in the magnitude of the dispersion of APD may be due to the geometric differences between the transmural plane in our simulations and the whole heart used in their experiments. Our simu-

lation represented only a small ( $8 \text{ mm} \times 8 \text{ mm}$ ) transmural plane, whereas Zabel *et al.*<sup>51</sup> placed several electrodes on the epicardium of both ventricles and one on the right ventricular endocardium. Thus, it is likely that the relatively large interelectrode distances in the experimental preparation provided the greater dispersion of APD. The  $g_{\text{ms}}(E_{\text{ff}})$  model showed a decrease in dispersion of  $\text{APD}_{90}$  from 8.3 to 1.1 ms, a result not observed in the experiments.

Transmural variation of  $\text{APD}_{90}$  has been measured in unstretched wedges excised from the canine ventricle. In arterially perfused LV wedge preparations, Yan *et al.*<sup>48</sup> measured  $\text{APD}_{90}$  at various wall depths. They found the maximal  $\text{APD}_{90}$  in the deep subendocardial M cells, averaging 260 ms at a basic cycle length of 1000 ms; the shortest  $\text{APD}_{90}$  (207 ms) occurred at the epicardium. The transmural dispersion of  $\text{APD}_{90}$  averaged 51 ms. At 15 mm Hg, our  $g_{\text{ms}}(E_{\text{cc}})$  model provided the largest dispersion of  $\text{APD}_{90}$  with 11.1 ms, or about 20% of the dispersion measured by Yan *et al.* At 5 mm Hg, the  $g_{\text{ms}}(E_{\text{ff}}, E_{\text{cc}})$  model showed only 4.6 ms of dispersion. Thus our model suggests that LV stretch may increase transmural dispersion of  $\text{APD}_{90}$  by 10%–20% via stretch-dependent currents in response to regionally heterogeneous strains. This increase in transmural dispersion of  $\text{APD}_{90}$  is likely to be an upper limit, though, since our model is only two-dimensional and electrically isotropic, whereas in the intact ventricle, cells are electrically coupled in three dimensions and electrotonus tends to reduce dispersion of  $\text{APD}_{90}$ .<sup>1,48</sup> Thus, mechanosensitive currents may be less important than the distribution of different ventricular cell types in determining the transmural dispersion of  $\text{APD}_{90}$ .

Overall, these results suggest that the stretch-dependent conductance is not a function of fiber or cross-fiber strain alone, because fiber strain [and, hence, the conductance obtained from the  $g_{\text{ms}}(E_{\text{ff}})$  model] is relatively uniform across the wall and fails to predict a transmural gradient of conductance. Similarly, the  $g_{\text{ms}}(E_{\text{cc}})$  model cannot reproduce the magnitude of epicardial action potential amplitude reduction since cross-fiber strain is relatively small at the epicardium but increases almost monotonically to a maximum value at the subendocardium. Only the model incorporating tensile strains in both the fiber and cross-fiber directions reproduced the magnitude of action potential amplitude reduction at the corresponding transmural locations.

The  $g_{\text{ms}}(E_{\text{ff}}, E_{\text{cc}})$  model relates cellular transmembrane stretch-dependent conductivities to the multidimensional deformation of myocardium. We used fiber and/or cross-fiber strains as the mechanical stimulus because these are the primary non-negative deformations of intact myocardium under passive loading.<sup>30</sup> Radial strain was omitted from the models because it is compressive

(negative) throughout the LV during passive loading, and stretch-inactivated channels have not been identified in cardiac cells.<sup>49</sup> Similarly, we omitted any influence of shear strain because no experimental evidence suggests mechanosensitive channels respond to shear deformation. Data to support the influence of specific components of the multidimensional strain tensor do not exist. Our results suggest more than a single component of the strain tensor is responsible for the mechanosensitivity of myocardium, but experimental observations to date have not identified the important strains. Time-dependent characteristics of mechanosensitive channels such as adaptation<sup>19</sup> and slow deactivation<sup>22</sup> were also not incorporated into our stretch-dependent conductivity models.

A large body of experimental results do, however, suggest that the mechanical stimulus is much more complex than the regionally varying stretch-dependent model we have proposed here. It is unclear whether mechanosensitive channels are activated by tension in the sarcolemma or stresses in the cytoskeletal proteins (or a combination of these).<sup>19</sup> Mechanosensitive channel activity has been measured in the absence of a cytoskeleton in membrane patches from *Escherichia coli* embedded in artificial bilayers.<sup>4,12</sup> In contrast, results from a series of patch-clamp experiments by Ruknudin *et al.*<sup>39</sup> suggest that mechanosensitive channels are in series with some component of the cytoskeleton. It has recently been suggested that mechanosensitive channels may not be located in the cell membrane, but in the T-tubules or some other internal membrane.<sup>6</sup> A regional variation in mechanosensitive channel expression, if it exists, could also confound the interpretation of tissue- and organ-level observations of mechanoelectric feedback.

Other experiments suggest the conductivity of a mechanosensitive channel may be affected by curvature of the membrane.<sup>7,28</sup> If a cardiac myocyte is assumed to be a circular cylinder that longitudinally lengthens and radially contracts as the ventricle is filled, the mechanosensitive channel activity would increase under passive loading based solely on the increased curvature due to the decrease in cross-sectional diameter. This scenario is further complicated by the data of Gerdes *et al.*<sup>18</sup> which shows the cross section of human LV myocytes is not circular but elliptical, with the major diameter more than twice the minor diameter. Gerdes *et al.*<sup>18</sup> collected additional data from the rat LV showing that 77% of the epimyocardial cells were oriented such that the major diameter is within 45° of the epicardial tangent plane. Thus, while curvature-sensitive channels *in vivo* may change their conductivity with changes in LV pressure, the amount of change may be dependent on the circumferential location of the channel on the cell membrane. Clearly, all models to date may be extreme simplifications of potentially complex relationships between the biophysics of mechanosensitive channels, the deforma-

tion of intact myocardium, and their combined effect on action potential morphology. Nevertheless, we have related regional changes in action potential amplitude to realistic heterogeneous strains of intact myocardium in a computationally tractable model.

Our choice of a maximum 30 mS/cm<sup>2</sup> for the stretch-dependent conductance did not block propagation in any of the regionally varying stretch-dependent conductance simulations. In all the simulations the area of maximum stretch-dependent conductance ( $g_{ms} = 30 \text{ mS/cm}^2$ ) was isolated to a small region (Figs. 4–6). The surrounding regions were capable of propagation and, hence, provided sufficient source current through the spatial coupling of the conductivity tensor to exceed the excitation threshold in the small regions of high conductance. This conductance is rather large, however, relative to the saturation conductances in the Beeler–Reuter model<sup>3</sup> and the maximal value (19 mS/cm<sup>2</sup>) suggested by experimental observations.<sup>38,41</sup> Action potential propagation was blocked at this value under the spatially uniform stretch-dependence conductance model (Fig. 3), providing a well-defined limiting value for our subsequent simulations.

All of the action potentials generated by the three models with regionally varying mechanical stimuli had amplitudes less than the baseline amplitude because the stretch-dependent current will tend to move the resting potential to a more depolarized quiescent state (i.e.,  $V_{RMP}$  will increase) and repolarize the cell during the plateau phase, decreasing the dome potential. The magnitude of these effects, however, will vary with the reverse potential of the mechanosensitive channel: a more negative reverse potential results in a smaller quiescent stretch-dependent current and a smaller increase in resting potential, but a larger decrease in the dome potential.<sup>34</sup>

### Limitations

Our results must be viewed in light of the limitations of the models. Action potential morphology is known to vary between epicardial, M, and endocardial cells.<sup>1</sup> We did not model this transmural variation though other investigators have done so successfully.<sup>9</sup> Fedida and Giles<sup>13</sup> have measured electrophysiological characteristics in rabbit ventricular cells and found the rest potential to be  $-80 \text{ mV}$ ; we used  $-84.5 \text{ mV}$ , the value in the Beeler–Reuter model.<sup>3</sup> The Beeler–Reuter model is also not specific to the rabbit but is instead derived from the analysis of mammalian ventricular cells from several species. More detailed ventricular action potential models exist; the most popular models improve upon the Beeler–Reuter representation of the sodium and potassium currents and include the effects of ion pumps, exchangers, and intracellular calcium transport.<sup>27</sup> These

mechanisms, though important for an essential description of cellular electrophysiology and analyses involving specific ionic currents, may not be fundamental to the regional analysis of mechano-electrical coupling we have conducted here. We have assumed that mechano-electric feedback in intact myocardium is governed by the activity of mechanosensitive channels, although it is not known whether these channels or alterations in intracellular calcium cycling, or the two combined, are the primary feedback mechanisms governing the electrical response to stretch.<sup>8</sup> It has been observed, however, that free cytosolic calcium is relatively low during diastole, thus the effect of stretch on the diastolic ventricle is likely dominated by mechanosensitive channel activity.<sup>42</sup> We considered only constant, sustained strains with our model, but myocardial strains change continuously throughout the cardiac cycle.<sup>47</sup> In the beating heart, mechanosensitive channels may contribute to arrhythmogenesis in patients with congestive heart failure (see Reiter<sup>32</sup> for a review), but their role in normal cardiac function is unknown. Bett and Sachs<sup>5</sup> propose that the intracellular calcium level may increase via direct calcium influx through mechanosensitive channels. Thus, a weak cell, stretched by its stronger neighbors, may accumulate more calcium, enhancing contractile force, resulting in a more uniform regional contraction.

It has been shown that accurately modeling the spatial variation of cellular electrophysiological events requires a resolution on the order of 50  $\mu\text{m}$  using a finite difference method.<sup>23</sup> A less refined discretization can result in significant errors in the fidelity of the action potential model.<sup>2</sup> Our propagation model, with a spatial resolution on the order of 760  $\mu\text{m}$  (the typical distance between two collocation points within a finite element), likely contains some discretization error. Rogers *et al.*<sup>36</sup> showed that a high-order finite element method converged comparably to a finite difference method at substantially higher spatial discretization for the FitzHugh–Nagumo equations, suggesting that our 760  $\mu\text{m}$  resolution may be equivalent to a more resolved finite difference grid. This analysis, however, has not yet been conducted using an ionic model of the action potential. Different action potential profiles between our spatially coupled model and the original spaced-clamped model<sup>3</sup> are likely the effect of the diffusive term in the cable equation. The maximum voltage during the upstroke of our baseline action potential (Fig. 3) is only 16.3 mV compared with 28 mV of the original model.<sup>3</sup> The action potential duration at 90% repolarization is slightly longer than that in the original model (287.3 vs 285 ms). The oscillations occurring immediately before and after the upstroke are likely caused by the cubic Hermite interpolation functions required by the collocation-Galerkin finite element method.<sup>2,37</sup> These oscillations are localized to within a few milliseconds of the upstroke, and we

believe they do not affect the results presented here, so their presence is of little consequence to the comparative value of our model.

The free parameters in our model likely could have been numerically optimized to give results nearly identical to the experimental observations. We feel such an effort is superfluous, however, because we do not propose that our model represents the mechanisms responsible for mechanosensitivity of myocardium. Instead, we propose that deformation of myocardium in multiple directions, not merely in a single direction as has been used in earlier models, is more likely to govern the mechanosensitive response of the intact ventricle.

The greatest conductivity in myocardium occurs in the direction of the long axis of the myofibers.<sup>25</sup> Here we have modeled the conductivity across the wall as isotropic, though this is only correct near the midwall region where the fibers are oriented in the circumferential direction, perpendicular to the transmural plane. At the epicardium and endocardium the conductivity is greater than what we have assumed because the fibers are more longitudinally oriented in these regions. This could affect the dispersion of APD through electrotonic influences. For the simulations we have performed, the smaller conductivity has the effect of reducing the stimulus current provided by the spatial coupling of the conductivity tensor, which could potentially lead to a subthreshold stimulus and failed propagation. With the spatially uniform stretch-dependent conductance model, propagation was blocked when  $g_{\text{ms}}=30 \text{ mS/cm}^2$  (Fig. 3). We did not observe failed propagation when using the regionally varying stretch-dependent conductance model, and the action potential with the lowest amplitude (approximately 66 mV at 15 mm Hg, Fig. 6) had a morphology similar to the  $g_{\text{ms}}=25 \text{ mS/cm}^2$  action potential (Fig. 3), suggesting all the propagated action potentials using this conductance model had adequate stimulus current. The isotropic conductivity tensor does not, however, allow for transmural variations in propagation velocity due to the transmural rotation of the fiber direction, hence, we did not investigate this aspect of the model.

The unloaded reference state for the model contained no residual stress, though residual stress is known to exist in the unloaded heart<sup>10,16,29</sup> and to affect resting sarcomere length.<sup>35</sup> The data of Costa *et al.*<sup>10</sup> show that residual strain is primarily tensile at the epicardium and compressive at the endocardium. Transformation of their data to a fiber-based coordinate system yields fiber strain of 0.038 at the epicardium, decreasing to zero at approximately 40% wall depth; cross-fiber strain is 0.052 at the epicardium, decreasing to zero at 20% depth. While it is not known if residual strain gives rise to stretch-dependent currents in the intact myocardium, present models of stretch-dependent conductance (including

those proposed here) would predict that the residual strain should increase the transmembrane rest potential of epicardial cells in the intact, unloaded ventricle.<sup>33,34,40</sup> The same cells should exhibit a reduced (more negative) rest potential in the stress-free state.

## CONCLUSIONS

We have conducted simulations of the effects of realistic myocardial strains on the action potential amplitude using different models of mechanosensitive conductance. Conductance models based on fiber strain or cross-fiber strain alone provided results similar to those observed experimentally, but failed to yield either the transmural gradient in action potential amplitude reduction or a sufficient magnitude of reduction at the epicardium. Only a model based on both fiber and cross-fiber strains simulated both effects. The same model nearly doubled the dispersion of action potential duration. These results suggest that the activity of mechanosensitive channels in the intact myocardium may be more complex than previously thought, with the channels responding to deformation other than lengthening along the long axis of the myocyte.

## ACKNOWLEDGMENTS

The authors are grateful to Dr. Jack Rogers of the University of Alabama at Birmingham (UAB) for extensive advice on the collocation-Galerkin finite element method. Dr. Andy Pollard and Dr. Delilah Huelsing (also of UAB) provided their implementation of the action potential model. Dr. Walt Baxter, Dr. Bill Karlon, and Reza Mazhari provided essential technical advice. Valuable improvements to the manuscript were suggested by Dr. Omer Berenfeld and Dr. Arkadii Perzov. This work was supported by NSF Grant No. BES-9634974 and by the National Biomedical Computation Resource (NIH Grant No. P 41 RR08605).

## NOMENCLATURE

$\alpha, \gamma$	mechanosensitive conductance parameters
$\beta$	mechanosensitive conductance scaling parameter
$E_{ij}$	Lagrangian Green's strain tensor components
$G_{ms}$	mechanosensitive channel saturation conductance
$g_{ms}(\cdot)$	stretch-dependent current conductance
$I_{ms}$	stretch-dependent current
$V_m$	cellular transmembrane voltage
$V_r$	mechanosensitive channel reverse potential
$V_{RMP}$	resting membrane potential
$\xi_i$	isoparametric finite element coordinate

## REFERENCES

- Antzelevitch, C., Z.-Q. Sun, Z.-Q. Zhang, and G.-X. Yan. Cellular and ionic mechanisms underlying erythromycin-induced long QT intervals and torsade de pointes. *J. Am. Coll. Cardiol.* 28(7):1836–1848, 1996.
- Beaumont, J., N. Davidenko, J. Davidenko, and J. Jalife. Self-sustaining spiral wave activity in a two-dimensional ionic model of cardiac ventricular muscle. In: *Computer Simulations in Biomedicine*. Boston, MA: Computational Mechanics, 1995, pp. 75–85.
- Beeler, G. W., and H. Reuter. Reconstruction of the action potential of ventricular myocardial fibers. *J. Physiol. (London)* 268(1):177–210, 1977.
- Berrier, C., A. Coulombe, C. Houssin, and A. Ghazi. A patch-clamp study of ion channels of inner and outer membranes and of contact zones of *E. coli*, fused into giant liposomes: Pressure-activated channels are localized in the inner membrane. *FEBS Lett.* 259(1):27–32, 1989.
- Bett, G. C. L., and F. Sachs. Cardiac mechanosensitivity and stretch-activated ion channels. *Trends Cardiovasc. Med.* 7(1):4–8, 1997.
- Bett, G. C. L., and F. Sachs. Whole-cell mechanosensitive currents in rat ventricular myocytes activated by direct stimulation. *J. Membr. Biol.* 173(3):255–263, 2000.
- Bowman, C. L., and J. W. Lohr. Curvature-sensitive mechanosensitive ion channels and osmotically evoked movements of the patch membrane (abstract). *Biophys. J.* 70(2):A365, 1996. Abstract Supplement for the Biophysical Society 40th Annual Meeting, 17–21 February 1996, Baltimore, Maryland.
- Calaghan, S. C., and E. White. The role of calcium in the response of cardiac muscle to stretch. *Prog. Biophys. Mol. Biol.* 71:59–90, 1999.
- Cates, A. W., and A. E. Pollard. A model study of intramural dispersion of action potential duration in the canine pulmonary conus. *Ann. Biomed. Eng.* 26(4):567–576, 1998.
- Costa, K. D., K. May-Newman, D. Farr, W. G. O'Dell, A. D. McCulloch, and J. H. Omens. Three-dimensional residual strain in midanterior canine left ventricle. *Am. J. Physiol.* 273:H1968–H1976, 1997.
- Craelius, W. Stretch-activation of rat cardiac myocytes. *Exp. Physiol.* 78(3):411–423, 1993.
- Delcour, A. H., B. Martinac, J. Adler, and C. Kung. Voltage-sensitive ion channel of *Escherichia coli*. *J. Membr. Biol.* 112(3):267–275, 1989.
- Fedida, D., and W. R. Giles. Regional variations in action potentials and transient outward current in myocytes isolated from rabbit left ventricle. *J. Physiol. (London)* 442:191–209, 1991.
- Franz, M. R. Current status of monophasic action potential recording: Theories, measurements, and interpretations. *Cardiovasc. Res.* 41:25–40, 1999.
- Franz, M. R., R. Cima, D. Wang, D. Proffitt, and R. Kurz. Electrophysiological effects of myocardial stretch and mechanical determinants of stretch-activated arrhythmias. *Circulation* 86(3):968–978, 1992; *ibid.* 86(5):1663, 1992.
- Fung, Y.-C. *Biodynamics: Circulation*. New York City: Springer, 1984.
- Gallagher, A. M., J. H. Omens, L. L. Chu, and J. W. Covell. Alterations in collagen fibrillar structure and mechanical properties of the healing scar following myocardial infarction. *Cardiovasc. Pathobiol.* 2(1):25–36, 1997.
- Gerdes, A. M., S. E. Kellerman, K. B. Malec, and D. D. Schocken. Transverse shape characteristics of cardiac myo-

- cytes from rats and humans. *Cardioscience* 5(1):31–36, 1994; *ibid.* 5(2):63, 1994.
- <sup>19</sup>Hamill, O. P., and D. W. McBride, Jr. Rapid adaptation of single mechanosensitive channels in *Xenopus oocytes*. *Proc. Natl. Acad. Sci. U.S.A.* 89(16):7462–7466, 1992.
- <sup>20</sup>Hansen, D. E., M. Borganelli, G. P. Stacy, Jr., and L. K. Taylor. Dose-dependent inhibition of stretch-induced arrhythmias by gadolinium in isolated canine ventricles. Evidence for a unique mode of antiarrhythmic action. *Circ. Res.* 69(3):820–831, 1991.
- <sup>21</sup>Hindmarsh, A. C. ODEPACK, a systematized collection of ODE solvers. In: *Scientific Computing: Applications of Mathematics and Computing to the Physical Sciences*, IMACS Transactions on Scientific Computation, edited by R. S. Stepleman. New York City: North-Holland, 1983, Vol. 1, pp. 55–64; available from <http://www.netlib.org/odepack>
- <sup>22</sup>Hu, H., and F. Sachs. Mechanically activated currents in chick heart cells. *J. Membr. Biol.* 154(3):205–216, 1996.
- <sup>23</sup>Joyner, R. W. Effects of the discrete pattern of electrical coupling on propagation through an electrical syncytium. *Circ. Res.* 50(2):192–200, 1982.
- <sup>24</sup>Kim, D. Novel cation-selective mechanosensitive ion channel in the atrial cell membrane. *Circ. Res.* 72(1):225–231, 1993.
- <sup>25</sup>Knisley, S. B., and B. C. Hill. Effects of bipolar point and line stimulation in anisotropic rabbit epicardium: Assessment of the critical radius of curvature for longitudinal block. *IEEE Trans. Biomed. Eng.* 42(10):957–966, 1995.
- <sup>26</sup>Lekven, J., K. Chatterjee, J. V. Tyberg, and W. W. Parmley. Reduction in ventricular endocardial and epicardial potentials during acute increments in left ventricular dimensions. *Am. Heart J.* 98(2):200–206, 1979.
- <sup>27</sup>Luo, C.-H., and Y. Rudy. A dynamic model of the cardiac ventricular action potential. I. Simulations of ionic currents and concentration changes. *Circ. Res.* 74(6):1071–1096, 1994.
- <sup>28</sup>Martinac, B., J. Adler, and C. Kung. Mechanosensitive ion channels of *E. coli*, activated by amphipaths. *Nature (London)* 348(6298):261–263, 1990.
- <sup>29</sup>Omens, J. H., and Y. C. Fung. Residual strain in rat left ventricle. *Circ. Res.* 66(1):37–45, 1990.
- <sup>30</sup>Omens, J. H., K. D. May, and A. D. McCulloch. Transmural distribution of three-dimensional strain in the isolated arrested canine left ventricle. *Am. J. Physiol.* 261:H918–H928, 1991.
- <sup>31</sup>Pollard, A. E., N. Hooke, and C. S. Henriquez. Cardiac propagation simulation. *Crit. Rev. Biomed. Eng.* 20(3–4):171–210, 1992.
- <sup>32</sup>Reiter, M. J. Contraction–excitation feedback. In: *Cardiac Electrophysiology: From Cell to Bedside*, 3rd ed. Philadelphia, PA: Saunders, 2000, Chap. 28, pp. 249–255.
- <sup>33</sup>Rice, J. J., R. L. Winslow, J. Dekanski, and E. McVeigh. Model studies of the role of mechano-sensitive currents in the generation of cardiac arrhythmias. *J. Theor. Biol.* 190(4):295–312, 1998.
- <sup>34</sup>Riemer, T. L., E. A. Sobie, and L. Tung. Stretch-induced changes in arrhythmogenesis and excitability in experimentally based heart cell models. *Am. J. Physiol.* 275:H431–H442, 1998.
- <sup>35</sup>Rodriguez, E. K., J. H. Omens, L. K. Waldman, and A. D. McCulloch. Effect of residual stress on transmural sarcomere length distributions in rat left ventricle. *Am. J. Physiol.* 264:H1048–H1056, 1993.
- <sup>36</sup>Rogers, J. M., M. S. Courtemanche, and A. D. McCulloch. Finite element methods for modeling impulse propagation in the heart. In: *Computational Biology of the Heart*, edited by A. V. Panfilov and A. V. Holden. West Sussex, England: Wiley, 1997, Chap. 7, pp. 217–234.
- <sup>37</sup>Rogers, J. M., and A. D. McCulloch. A collocation-Galerkin finite element model of cardiac action potential propagation. *IEEE Trans. Biomed. Eng.* 41(8):743–757, 1994.
- <sup>38</sup>Ruknudin, A., F. Sachs, and J. O. Bustamante. Stretch-activated ion channels in tissue-cultured chick heart. *Am. J. Physiol.* 264:H960–H972, 1993.
- <sup>39</sup>Ruknudin, A., M. J. Song, and F. Sachs. The ultrastructure of patch-clamped membranes: A study using high-voltage electron microscopy. *J. Cell Biol.* 112(1):125–134, 1991.
- <sup>40</sup>Sachs, F. Modeling mechanical–electrical transduction in the heart. In: *Cell Mechanics and Cellular Engineering*, edited by V. C. Mow, F. Guilak, R. M. Hochmuth, and R. Tran-Son-Tay. New York City: Springer, 1994, Chap. 18, pp. 308–328.
- <sup>41</sup>Sigurdson, W., A. Ruknudin, and F. Sachs. Calcium imaging of mechanically induced fluxes in tissue-cultured chick heart: Role of stretch-activated ion channels. *Am. J. Physiol.* 262:H1110–H1115, 1992.
- <sup>42</sup>Taggart, P., and P. M. I. Sutton. Cardiac mechanoelectric feedback in man: Clinical relevance. *Prog. Biophys. Mol. Biol.* 71:139–154, 1999.
- <sup>43</sup>Van Leuven, S. L., L. K. Waldman, A. D. McCulloch, and J. W. Covell. Gradients of epicardial strain across the perfusion boundary during acute myocardial ischemia. *Am. J. Physiol.* 267:H2348–H2362, 1994.
- <sup>44</sup>Vetter, F. J., and A. D. McCulloch. Three-dimensional analysis of regional cardiac function: A model of rabbit ventricular anatomy. *Prog. Biophys. Mol. Biol.* 69(2/3):157–183, 1998.
- <sup>45</sup>Vetter, F. J., and A. D. McCulloch. Three-dimensional stress and strain in passive rabbit left ventricle: A model study. *Ann. Biomed. Eng.* 28(7):781–792, 2000.
- <sup>46</sup>Vetter, F. J., J. M. Rogers, and A. D. McCulloch. A finite element model of passive mechanics and electrical propagation in the rabbit ventricles. In: *Computers in Cardiology 1998*. New York City: Institute of Electrical and Electronics Engineers, 1998, Vol. 25, pp. 705–708.
- <sup>47</sup>Waldman, L. K. Multidimensional measurement of regional strains in the intact heart. In: *Theory of Heart: Biomechanics, Biophysics, and Nonlinear Dynamics of Cardiac Function*, edited by L. Glass, P. Hunter, and A. McCulloch. New York City: Springer, 1991, Chap. 7, pp. 145–174.
- <sup>48</sup>Yan, G.-X., W. Shimizu and C. Antzelevitch. Characteristics and distribution of M cells in arterially perfused canine left ventricular wedge preparations. *Circulation* 98(18):1921–1927, 1998.
- <sup>49</sup>Yang, X. C., and F. Sachs. Mechanically sensitive, nonselective cation channels. *Exs* 66:79–92, 1993.
- <sup>50</sup>Zabel, M., B. S. Koller, F. Sachs, and M. R. Franz. Stretch-induced voltage changes in the isolated beating heart: Importance of the timing of stretch and implications for stretch-activated ion channels. *Cardiovasc. Res.* 32(1):120–130, 1996.
- <sup>51</sup>Zabel, M., S. Portnoy, and M. R. Franz. Effect of sustained load on dispersion of ventricular repolarization and conduction time in the isolated intact rabbit heart. *J. Cardiovasc. Electrophysiol.* 7(1):9–16, 1996.